Research Article Vol. 62, No. 5 / 10 February 2023 / Applied Optics 1183

applied optics

Optical design and precision analysis of a single-line-array pendulum sweep high-resolution mapping camera

Yazhen Cui,[1,2,3] Chunyu Liu,[1,3,*] Shuai Liu,[1,3] Minglin Xu,[1,3] and Peng Xie[1,3]

[1]Changchun Institute of Optics, Fine Mechanics and Physics, Chinese Academy of Sciences, Changchun, Jilin 130033, China
[2]University of Chinese Academy of Sciences, Beijing 100049, China
[3]Key Laboratory of Space-Based Dynamic & Rapid Optical Imaging Technology, Chinese Academy of Sciences, Changchun, Jilin 130033, China
*Corresponding author: mmliucy@163.com

Received 24 November 2022; revised 28 December 2022; accepted 28 December 2022; posted 3 January 2023; published 2 February 2023

With the improvement of the satellite resolution, it is urgent to develop the single-line-array mapping camera. However, the camera accuracy is influenced by the satellite attitude's rapid maneuvering during the imaging process. In our study, a coaxial four-mirror optical system with a field bias with a focal length of 7050 mm, F-number of 10.8, field of view of 1.2°, and spectral range of 450–800 nm is designed. By combining mathematical modeling and ray tracing, the offset of the camera interior orientation elements caused by the misalignment of the secondary mirror is derived. The simulation results show that the maximum relative error does not exceed 2.119%. Besides, a desensitization design method based on the magnification parameter control method is proposed, and the results show that the sensitivity of camera interior orientation elements to the secondary mirror is reduced, indicating the effectiveness of the system desensitization design, which is of great significance for the improvement of camera accuracy.

https://doi.org/10.1364/AO.481706

1. INTRODUCTION

Satellite mapping is mainly divided into three mapping systems: three-line-array, two-line-array, and single-line-array [1]. The resolution and precision of satellite cameras need to be improved to meet the improvement requirements of the satellite mapping scale index. On one hand, with the improvement of camera spatial resolution, the weight and volume of the camera will increase accordingly. Traditional single-lens three-line-array mapping cameras increase the difficulty of optical design [2], and conventional satellite platforms have a problem carrying mapping cameras consisting of two or three independent lenses [3]. The single-line-array pendulum sweep mapping camera is composed of a single lens, which is maneuvered by satellite attitude or swept back and forth by the camera while pushing and scanning the ground at a certain rendezvous angle to achieve target positioning [4]. It dramatically reduces the weight and volume of the satellite and is of great significance for developing microsatellite mapping.

On the other hand, the precision of the mapping camera interior orientation elements is one of the key indicators to ensure the satellite mapping accuracy [3]. The factors affecting the precision of the camera interior orientation elements (and the camera accuracy) mainly include the camera's ground calibration and on-orbit calibration [5–7]. Unlike multi-line-array mapping cameras, which push and sweep the ground at a fixed angle, the thermal stability of the single-line-array mapping camera is affected during camera flipping [8], so the on-orbit calibration of the camera internal orientation elements becomes more complicated.

The thermal environmental factors that affect the camera interior orientation elements are mainly reflected in the spatial position misalignment of the optical elements in the optical system. The changes in the camera interior orientation elements caused by the above errors should be minimized as soon as possible to achieve high-precision positioning of the high-resolution single-linear-array pendulum sweep mapping camera. An optical system with low sensitivity of interior orientation elements should be obtained to improve the satellite's mapping accuracy.

There are many desensitization design methods of the optical system, mainly divided into direct optimization method, aberration control method, parameter control method, etc. Among them, the parameter control method takes control of parameters that have clear laws or mathematical relationships with error sensitivity as the core, including the light angle optimization method [9–11], the optical element shape parameter control method [12,13], the off-axis control method [14], and the optical path control method [15]. In comparison, this method is more efficient and straightforward to implement. When the optical component deviation of the previous part of the system passes through the optical component of the latter part, the camera accuracy will be further affected by the magnification of

the latter part. Therefore, the magnification parameter control method is used to reduce the error sensitivity of camera precision to an optical element for the system.

The camera optical system determines the external dimensions and layout of the camera [16]. Considering the light and miniaturization requirements of cameras, based on the single-line-array satellite mapping requirements with a scale of 1:5000, this paper designs a coaxial four-mirror optical system with a field bias. Additionally, taking this system as the research object, the theoretical expression of camera interior orientation elements caused by the various types of misalignment of the secondary mirror is derived by combining mathematical modeling and ray tracing. Then the system desensitization design method of adjusting the magnification of the third or fourth mirror is proposed, which is of great significance for developing a single-line-array pendulum sweep high-resolution mapping camera.

2. OPTICAL SYSTEM DESIGN

A. Determination of Optical Parameters

According to the requirements that the ground pixel resolution at the track of 500 km of the camera is better than 0.5 m, the calculation of Eq. (1) shows that the system's focal length is 7000 mm:

$$f' = \frac{H}{\mathrm{GSD}} \cdot a. \tag{1}$$

In Eq. (1), f' is the focal length of the system. H is the orbital altitude, and its value is 500 km. a is the pixel size of the detector, which is 7 μm × 7 μm. GSD is the ground sampling distance, and its value is not less than 0.5 m. The system's focal length was determined to be 7050 mm to leave a certain margin.

According to the requirements that the ground width of the camera is not less than 10 km at the track of 500 km, the half-field angle of the system can be calculated from Eq. (2), which is not less than 0.57°:

$$\omega = \arctan\frac{W}{2H} = 0.57°. \tag{2}$$

In Eq. (2), ω is the half-field angle of the system. W is the ground width, and its value is not less than 10 km. Thus, the total field of view of the system was determined to be 1.2°.

The relative aperture of the optical system is closely related to the camera's signal-to-noise ratio (SNR). The SNR of the camera is determined by the noise characteristics of the detector, and it can be defined as the ratio of signal power to noise power, expressed as shown in Eq. (3) [17]:

$$R_{\mathrm{SN}} = \frac{S_e}{N_e} = \frac{S_e}{\sqrt{S_e + \sigma_R^2 + D_e}}. \tag{3}$$

In Eq. (3), S_e is the number of signal photoelectrons, and the number of signal photoelectrons in the integration period can be calculated from Eq. (4). N_e is the number of noise photoelectrons. σ_R and D_e are the readout noise and dark current of the detector, respectively. As can be seen by consulting the manual of the GSENSE5130 sensor, $\sigma_R = 1.6e^{-1}$, $D_e = 3e^{-1}$/s/pix:

$$S_e = \frac{\pi AMt}{4hc/\lambda} L_0 \tau \eta \cdot \left(\frac{D}{f'}\right)^2. \tag{4}$$

In Eq. (4), A is the size of a single pixel, M is the integral progressions of the detector, $t \approx \frac{\mathrm{GSD}}{v}$ is the exposure time, and v is the operating speed. L_0 is the radiance at the pupil of the optical system, which can be calculated by an atmospheric simulation. τ is the reflectance of the optical system, which is determined by the reflectance of the system mirror surface. η is the quantum efficiency of the detector. $\frac{D}{f'}$ is the relative aperture of the optical system, h is Planck's constant, c is the light speed, and λ is the center wavelength.

The single-line-array pendulum sweep high-resolution mapping camera system is expected to use five mirrors with a reflectance of 0.95 in the 450–800 nm spectral range. Each mirror will be coated with a reflective coating with a reflectance of 0.995. When the relative aperture of the system is 1/10.8, the radial brightness value of the optical system at the pupil and the corresponding camera SNR estimation values when the solar height angle is greater than 70°, and the ground object reflectance is greater than 0.65, while the sun height angle is greater than 20°, and the ground object reflectance is greater than 0.05, respectively, are as shown in Table 1.

In general, the modulation transfer function (MTF) of the camera is determined by the MTF value of three parts. They are optical system design, processing and assembly, and detector sampling. According to the requirement that the MTF of the camera at the Nyquist frequency is greater than 0.12, it can be seen from Eq. (5) that the MTF value of the camera optical system design should be greater than 0.3 at the Nyquist frequency [18]:

$$\mathrm{MTF} = \mathrm{MTF}_{\mathrm{design}} \cdot \mathrm{MTF}_{\mathrm{manufacture}} \cdot \mathrm{MTF}_{\mathrm{detector}}. \tag{5}$$

In Eq. (5), MTF is the MTF value of the camera. $\mathrm{MTF}_{\mathrm{design}}$ is the MTF value of the camera optical system design. $\mathrm{MTF}_{\mathrm{manufacture}}$ is the MTF value of optical system processing and assembly, and it is better than 0.8 according to the experience of processing and assembly. $\mathrm{MTF}_{\mathrm{detector}}$ is the MTF value of detector sampling, which is generally 0.5.

Table 1. Estimation of the Camera SNR

Detector	Maximum Radiant Brightness W/(sr · cm²)	Minimum Radiant Brightness W/(sr · cm²)	Maximum SNR	Minimum SNR
Panchromatic	6.234906×10^{-3}	4.067499×10^{-4}	55.0993	43.2438
Multispectral–B1	1.167390×10^{-3}	1.272638×10^{-4}	46.5512	36.9241
Multispectral–B2	1.021462×10^{-3}	7.520184×10^{-5}	46.5957	35.2627
Multispectral–B3	1.003343×10^{-3}	5.330783×10^{-5}	47.2316	34.4813
Multispectral–B4	2.167323×10^{-3}	8.826453×10^{-5}	51.4659	37.5626

Table 2. Design Parameters of the Optical System

Parameters	Value
Spectral range	450–800 nm
Focal length	7050 mm
Relative aperture	1/10.8
Field of view	1.2°
MTF	>0.3 at 71 lp/mm
Distortion	<0.05%

Combined with the above analysis, the design parameters of the single-line-array pendulum sweep high-resolution mapping camera optical system can be shown in Table 2.

B. Optical System Design

According to the optical design parameters in Table 2, the single-line-array pendulum sweep high-resolution mapping camera system is an optical system with a long focal length and minor field of view. Reflective systems are preferred for long focal length optical systems [19]. Additionally, due to the small field of view, a coaxial reflective optical system is selected. A coaxial four-mirror optical system is proposed to minimize the camera's weight and volume. The system takes a coaxial two-mirror optical system as the initial structure for further design and optimization. On this basis, the third and fourth mirrors are added to correct the large number of aberrations caused by the system's large aperture and long focal length. At the same time, the folding mirror is added to the optical path to achieve the folding of the optical path, thereby compressing the system's volume. In the early design stage, it is important to do an excellent job of the distance constraint between the folding, third and fourth mirrors. First, restrict the distance between the folding and third mirrors so that it is smaller than the half-aperture of the primary mirror to ensure the position of the third mirror. Secondly, restrict the distance between the fourth mirror and the image plane so that it is smaller than the primary mirror's full aperture to ensure the image plane's position. Thirdly, restrict the distance between the third and fourth mirrors so that it is smaller than the primary mirror's full aperture to ensure the fourth mirror's position. In the later stage of design, the main task is to make the imaging position of the primary and secondary mirror fall on the folding mirror and set the field bias to reduce the impact of the primary occlusion and secondary occlusion on the imaging quality of the system.

Under the above design ideas, the system is optimized by the optical design software. Set the distance between mirrors, the curvature of mirrors except for the folding mirror, and the quadric surface coefficients of the primary, secondary, and third mirrors as variables for further design and optimization. After several iterations of optimization, the optical system structure shown in Fig. 1 is obtained. The MTF and spot diagram of the system are shown in Figs. 2 and 3, respectively. As seen in Fig. 2, the MTF of the system is close to the diffraction limit. As seen in Fig. 3, the maximum RMS spot radius of the system is 7.633 um, which means that the system has excellent imaging quality. The relative distortion of the system is shown in Fig. 4, and it can be seen that the maximum relative distortion of the system is 0.0133%, which meets the requirements of the design index.

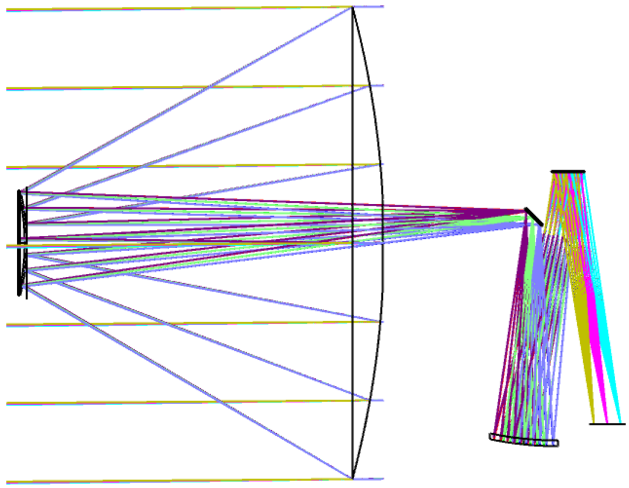

Fig. 1. Optical system structure.

3. PRECISION ANALYSIS

A. Types of Optical Component Misalignment and Camera Interior Orientation Elements

Optical element misalignment refers to the position error of the optical element, which can be roughly summarized into eccentricity and tilt, and divided into X, Y, and Z in three directions, respectively. Typically, a single optical element misalignment in an optical system has five degrees of freedom, excluding the tilt in the Z direction [20]. In practice, various types of misalignment often coexist. The position error of a single class and a single direction is used as the research object, and the offset of optical components is analyzed in the meridian to facilitate the analysis; that is, the eccentricity and tilt offset of the optical elements are studied in the Y and X directions, respectively.

The internal orientation elements of the mapping camera are the parameters that describe the relevant position between the photographic center and the image plane [21], including the principal point and the principal distance of the camera. The camera's principal point is also called the image principal point. It is to be distinguished from the optical system's principal point, later called the image principal point. As shown in Fig. 5, the principal distance is defined as the vertical distance from the center of photography S to the image plane, denoted by f, assuming that this vertical feet is O, and the image principal point is defined as the position of the point O in the image plane coordinate system, represented using (x_0, y_0). Here the center of photography can be understood as the node of the camera optical system. In the same medium, the primary point and node of the system coincide. Therefore, the principal distance can be expressed by the vertical distance from the principal point of the system to the image plane, and the image principal point can be described by the intersection (vertical feet) of the principal point of the system and the image plane. When the system is not disturbed by optical components, among the many rays incident from infinity on the system parallel to the optical axis, the ray with a 0 aperture and 0 field of view passes precisely through the principal point S of the system and is imaged in the center O of the image plane, as shown in Fig. 6. Suppose the plane coordinate system is established with the center of the image plane as the origin. In this case, the coordinate

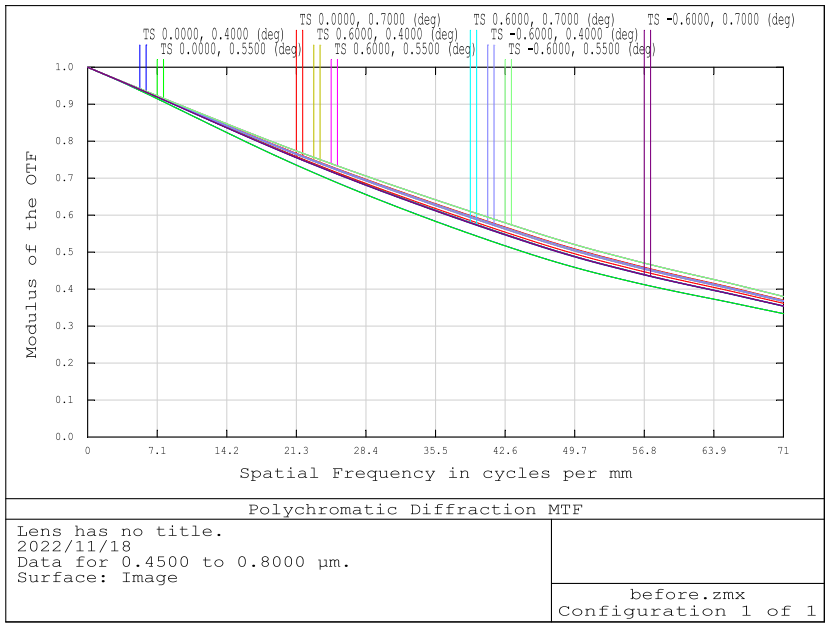

Fig. 2. MTF of the optical system.

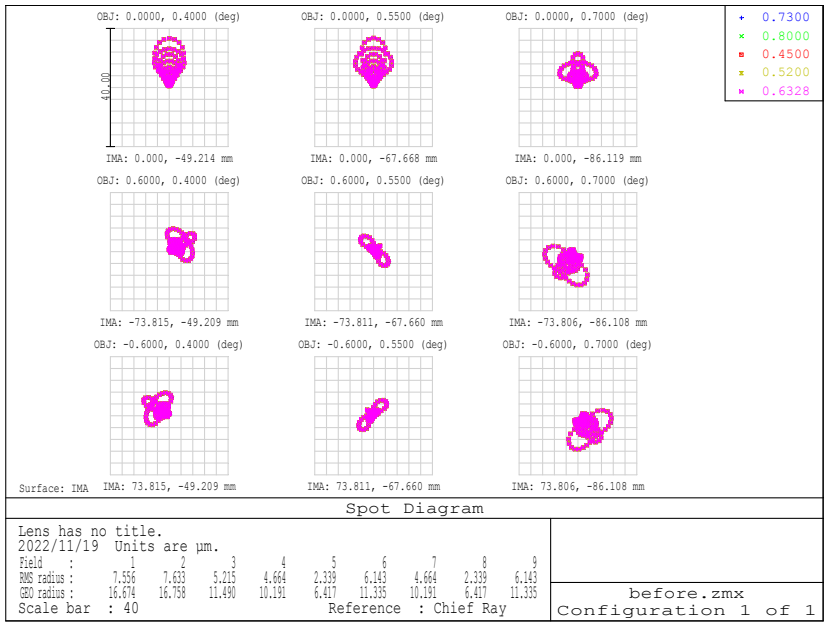

Fig. 3. Spot diagram of the optical system.

of the camera image principal point is $(x_0, y_0) = (0, 0)$, and the principal distance f is the distance from the principal point of the system to the image plane (focal plane), which is equal to the length of the system focal length.

For the system designed in Section 2.B, taking the primary mirror as the reference, by comparing the effect of the position error of these mirrors on the MTF of the system, it can be seen that the position error of the secondary mirror is the main reason for the accuracy of the camera interior orientation elements. Therefore, the following content of this paper will focus on the secondary mirror misalignment and introduces an analysis method for the influence of the optical component misalignment on the precision of interior orientation elements of the mapping camera. Meanwhile, it will provide a sensitivity idea to reduce the sensitivity of the secondary mirror misalignment to the interior orientation elements of the mapping camera.

B. Influence of Secondary Mirror Eccentricity Offset of the Coaxial Four-Mirror Optical System on the Camera Image Principal Point

From Section 2.B, it can be seen that the structure of the coaxial four-mirror optical system is composed of the primary, secondary, folding, third, and fourth mirrors, and its aperture diaphragm is on the primary mirror. Since the Z-direction eccentricity of the secondary mirror does not affect the camera image principal point, it is only necessary to analyze the

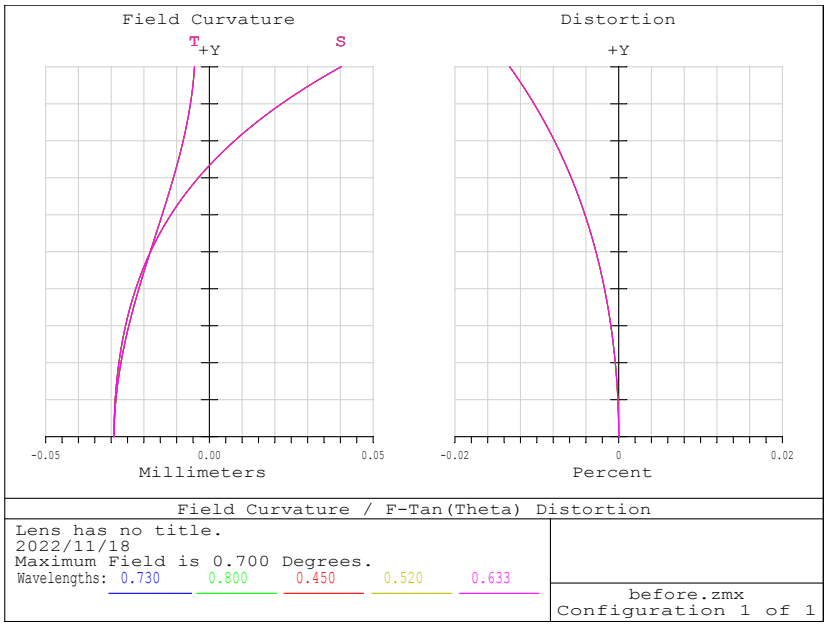

Fig. 4. Field curvature and distortion of the optical system.

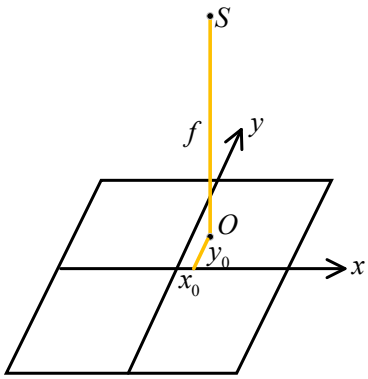

Fig. 5. Interior orientation elements in the mapping camera.

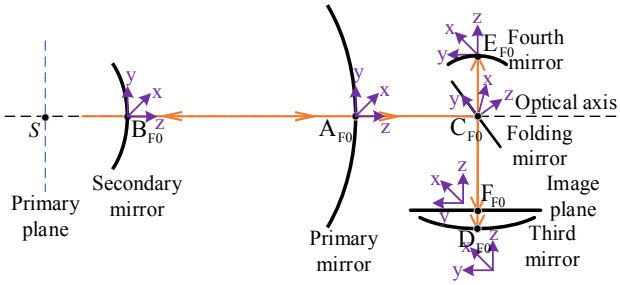

Fig. 6. Ray tracing with a 0 aperture and 0 field of view of the coaxial four-mirror optical system.

influence of the secondary mirror's X- and Y-direction offset on the camera image principal point. A right-handed coordinate system is established on the surface using the surface vertex of each optical element as the origin to facilitate the analysis. On this basis, the quadric equation for each mirror can be expressed as

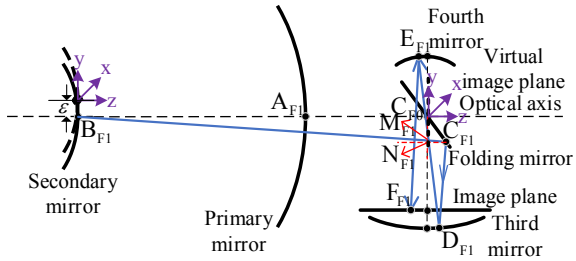

Fig. 7. Ray tracing produced by the secondary mirror Y eccentric offset of the coaxial four-mirror optical system.

$$y^2 = a_1 z + a_2 z^2. \tag{6}$$

In Eq. (6), $a_1 = 2R$, $a_2 = K - 1$, R is the vertex curvature radius of the surface, and K is the quadric constant.

In addition, the mirror surface is usually an arbitrary curved surface, which can often be defined as [15]

$$z = \frac{cy^2}{1 + \sqrt{1 - (1 + K)c^2 y^2}}. \tag{7}$$

In Eq. (7), z is the vector height of the surface parallel to the optical axis, and $c = 1/R$ is the vertex curvature of the surface.

As shown in Fig. 7, if the secondary mirror is eccentric ε in the Y direction, the coordinate of B_{F1} in the eccentric secondary mirror coordinate system is $(z_{21}, y_{21}) = (\Delta z, -\varepsilon)$. [$\Delta z$ can be calculated from Eq. (7)]. On this basis, if the equation of the fourth mirror outgoing ray can be determined by combining mathematical modeling and ray tracing, the offset of the camera image principal point when the secondary mirror is eccentric ε in the Y direction can be obtained.

In Eq. (7), the normal slope of the incident ray at a point on the mirror surface is obtained by biasing y to z, as shown in Eq. (8):

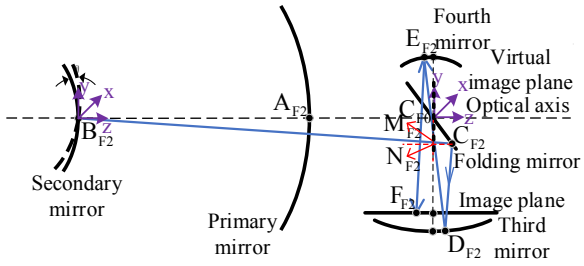

Fig. 8. Ray tracing produced by the secondary mirror X-tilt offset of the coaxial four-mirror optical system.

$$k_{\text{nor}} = -\frac{2y}{a_1 + 2a_2 z}. \tag{8}$$

Assuming that the angle between the normal and the optical axis at a point on the mirror surface is θ, there is

$$\tan\theta = \frac{|k_{\text{nor}} - k_{\text{in}}|}{\sqrt{1 + k_{\text{nor}} k_{\text{in}}}} = \frac{|k_{\text{out}} - k_{\text{nor}}|}{\sqrt{1 + k_{\text{out}} k_{\text{nor}}}}. \tag{9}$$

In Eq. (9), k_{in} and k_{out} represent the slope of the incident and outgoing ray at a point on the mirror surface, respectively. As shown in Fig. 7, the incident ray at the point B_{F1} on the secondary mirror surface is parallel to the optical axis. Hence, the slope of the incident ray at the point B_{F1} is $k_{\text{in}} = 0$.

The linear equation $B_{F1}C_{F1}$ can be established using the coordinates of the point B_{F1} in the virtual image plane coordinate system and the slope of the line $B_{F1}C_{F1}$, where the slope of the line $B_{F1}C_{F1}$ is the slope of the outgoing ray at that point B_{F1}, which can be calculated from the Eq. (9). For this equation, if $z = 0$, the coordinates M_{F1} of the ray incident on the surface of the virtual image plane can be obtained, and the line segment $|C_{F0}M_{F1}| = \frac{2d_2}{R_2}\varepsilon$ can be known. Then the distance from the point C_{F0} to N_{F1} can be determined using geometric relationships so that the coordinates of the incident ray on the surface C_{F1} of the folding mirror can be obtained. According to the above method and process, the solution is face-by-face. Finally, the offset of the camera image principal point when the secondary mirror is eccentric ε in the Y direction can be obtained, which can be expressed as Eq. (10):

$$\Delta y = \varepsilon\left[\frac{-4(d_2 + d_3)(d_4 + d_5)}{R_2 R_3} + \frac{2(d_2 + d_3 + d_4 + d_5)}{R_2} + \frac{4(d_2 + d_3 + d_4)d_5}{R_2 R_4} - \frac{8(d_2 + d_3)d_4 d_5}{R_2 R_3 R_4}\right]. \tag{10}$$

In Eq. (10), d_2, d_3, d_4, and d_5 are the distances between the secondary to the folding mirror, the folding mirror to the third mirror, the third mirror to the fourth mirror, and the fourth mirror to the image plane, respectively, which are greater than 0.

C. Influence of Secondary Mirror Tilt Offset of the Coaxial Four-Mirror Optical System on the Camera Image Principal Point

As shown in Fig. 8, if the secondary mirror is tilted ω in the Y direction, the coordinate B_{F2} in the tilted secondary mirror coordinate system is $(z_{22}, y_{22}) = (0, 0)$.

The linear equation $B_{F2}C_{F2}$ can be established in the virtual image plane coordinate system. According to the law of reflection and geometric relations, the slope of the line $B_{F2}C_{F2}$ is $k_{\text{out}} = -\tan 2\omega$. The coordinate $(z'_{22}, y'_{22}) = (-d_2\cos\omega, d_2\sin\omega)$ of the point B_{F2} in the virtual image plane coordinate system can be obtained using the coordinate transformation. Similarly, the line segment $|C_{F0}M_{F2}| = -d_2\tan\omega$ can be known and, by using the same method and process, the offset Δy of the camera image principal point can be obtained when the secondary mirror is tilted in the X direction, which can be expressed as Eq. (11):

$$\Delta y = \tan\omega\left[\frac{2(d_2 + 2d_3 - R_3)}{R_3 R_4} + \frac{2(d_2 + 2d_3 - R_3)(d_4 + d_5)}{R_3} - \frac{(d_2 + 2d_3)d_5}{R_4} - (d_2 + 2d_3)\right]. \tag{11}$$

To verify the offset expression of the camera image principal point caused by the secondary mirror offset of the coaxial four-mirror optical system derived above, the system designed in Section 2.B is given Y-eccentricity and the X-tilt offset of the secondary mirror, respectively. The results are shown in Table 3. It can be seen from Table 3 that the relative error of the camera image principal point offset caused by the offset of the secondary mirror does not exceed 1.07%, which verifies the correctness of the theoretical derivation.

D. Influence of Secondary Mirror Misalignment of the Coaxial Four-Mirror Optical System on the Camera Principal Distance

When there is a misalignment of the secondary mirror in the coaxial four-mirror optical system, the camera principal distance will change as the camera image principal point or the system focal length changes. When the secondary mirror produces Y-direction eccentricity or the X-direction tilt offset, the system's focal length does not change. Still, due to the camera image principal point changes, the camera principal distance will also change. When the secondary mirror produces a Z-direction eccentricity offset, the focal length of the system changes; therefore, the camera's primary distance also varies. The folding mirror is omitted to study the effect of the misalignment of the secondary mirror in the coaxial four-mirror optical system on the camera principal distance to facilitate the analysis.

The change of the camera principal distance in which the secondary mirror in the coaxial four-mirror optical system produces eccentricity or tilt offset in the X or Y direction can be obtained by the offset of the camera image principal point caused by these offsets. The change from the camera image principal point G_0 to G_1 can be regarded as the deflection of

Table 3. Analysis of the Camera Image Principal Point Offset When the Secondary Mirror in the Coaxial Four-Mirror Optical System Is Offset

Offset	Value of Calculation/mm	Value of Tracing/mm	Relative Error
Y/0.1 mm	0.95936033598	0.95935916630	0.0001219%
X/0.1°	2.32779112449	2.30299294460	1.065%

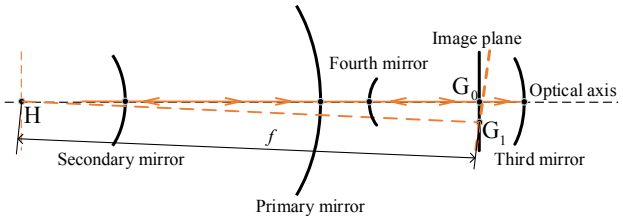

Fig. 9. Change of the camera principal distance with X- or Y-direction eccentricity or the tilt offset generated by the secondary mirror of the coaxial four-mirror optical system.

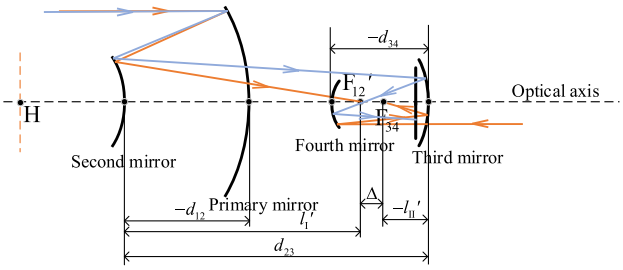

Fig. 10. Change of the camera principal distance with a Z-direction eccentricity offset generated by the secondary mirror of the coaxial four-mirror optical system.

the image plane. Therefore, according to the definition of the camera principal distance, it can be expressed as the distance $|HG_1|$ from the system principal point H to the camera image principal point G_1. The following relationship can be obtained from Fig. 9:

$$|HG_1|^2 = |HG_0|^2 + |G_0G_1|^2. \tag{12}$$

In Eq. (12), $|HG_0|$ is the length of the system focal length, and $|G_0G_1|$ is the offset size of the camera image principal point. According to the offset of the camera image principal point described in Sections 3.B and 3.C, respectively, the offset of the camera principal distance can be obtained.

Suppose the coaxial four-mirror optical system studied in this paper is divided into two mirror groups, as shown in Fig. 10. In this case, the primary and secondary mirrors form the first mirror group, and the third and fourth mirrors form the second. Assuming that the focal length of the first mirror group is f'_{12}, the focal length of the second mirror group is f'_{43}, and the optical interval between the two mirror groups is Δ is

$$f' = -\frac{f'_{12}f'_{43}}{\Delta}. \tag{13}$$

In Eq. (13), $\Delta = d_{34} - [l'_{\mathrm{I}} - (d_{23} + d_{12} + d_{34})] - (-l'_{\mathrm{II}})$ is the distance between the image focus of the first mirror group and the object focus of the second mirror group. Among them, l'_{I} and l'_{II} are the image distances of the first and second mirror groups, respectively. In addition, f'_{12}, f'_{43}, l'_{I}, and l'_{II} can be obtained by the Gaussian optical formula. The system's corresponding focal length, i.e., the camera's principal distance, can be calculated from this.

The system designed in Section 2.B is also given Y-eccentricity, X-tilt, and Z-eccentric offset of the secondary mirror to verify the change of the camera image principal distance caused by the secondary mirror offset analyzed above. The results are shown in Tables 4 and 5. It can be seen that the relative error of the camera principal distance offset caused by the offset of the secondary mirror does not exceed 2.119% at most, which proves the correctness of the theoretical analysis.

Table 4. Analysis of the Camera Principal Distance Offset When the Secondary Mirror in the Coaxial Four-Mirror Optical System Has Eccentricity or Tilt Offset in the X or Y Direction

Offset	Value of Calculation/mm	Value of Tracing/mm	Relative Error
Y/0.1 mm	0.00006527462	0.00006527446	0.0002451%
X/0.1°	0.00038429862	0.00037615429	2.1119%

Table 5. Analysis of the Camera Principal Distance Offset When the Secondary Mirror in the Coaxial Four-Mirror Optical System Has a Z-Direction Eccentricity Offset

Z-Direction Eccentricity Offset/um	Value of Calculation/mm	Value of Tracing/mm	Relative Error
−2	−4.29124651440	−4.29124700000	0.00001132%
−1	−2.14627433420	−2.14627400000	0.00001557%
0	0.00000000000	0.00000000000	——
1	2.14757770633	2.14757800000	0.00001368%
2	4.29645996765	4.29646000000	0.0000007500%

4. DESENSITIZED DESIGN

A. Desensitized Design

Considering that there is a specific relationship between the principal distance and the image principal point of the camera, the subsequent desensitization design focuses on the change of the camera image principal point to reduce the influence of the secondary mirror misalignment on the camera's image principal point and principal distance. The magnification of the third or fourth mirror further affects the deviation of rays on the folding mirror surface caused by the offset of the secondary mirror. The smaller the magnification of the third or the fourth mirror, the less is the effect of the secondary mirror on the camera image principal point. Therefore, the desensitization design can be obtained by adjusting the magnification of the system's third or fourth mirror. The gaze is shifted to control the magnification product of the third and fourth mirror to control the magnification of the third or fourth mirrors uniformly. The product is reduced to achieve the purpose of desensitizing the system.

First, the magnification of the system's third or fourth mirror is characterized, which can be calculated using the optical path shown in Fig. 11, obtained by using the Gaussian optical formula, and expressed as Eqs. (14) and (15), respectively:

$$\beta_T = -\frac{R_3}{2\left[\frac{R_2\left(\frac{R_1}{2}-d_{12}\right)}{2\left(\frac{R_1}{2}-d_{12}\right)-R_2} - d_{23}\right] - R_3}, \tag{14}$$

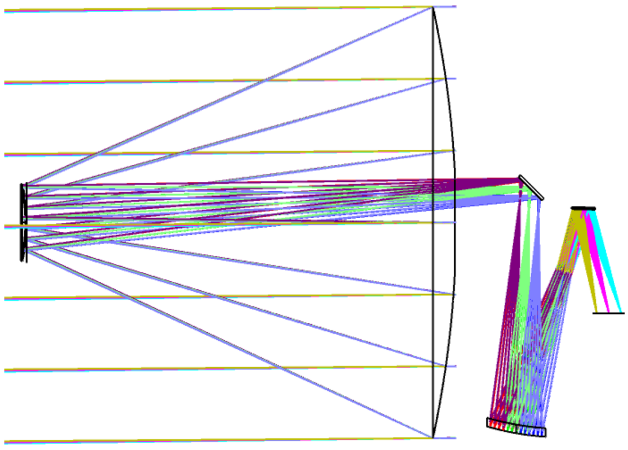

Fig. 11. Desensitized system structure.

$$\beta_F = -\frac{R_4}{2\left\{R_3\left[\frac{R_2\left(\frac{R_1}{2}-d_{12}\right)}{2\left(\frac{R_1}{2}-d_{12}\right)-R_2}-d_{23}\right]\Big/2\left[\frac{R_2\left(\frac{R_1}{2}-d_{12}\right)}{2\left(\frac{R_1}{2}-d_{12}\right)-R_2}-d_{23}\right]-d_{34}\right\}-R_4}. \quad (15)$$

The formula $\frac{R_2(\frac{R_1}{2}-d_{12})}{2(\frac{R_1}{2}-d_{12})-R_2}$ in Eqs. (14) and (15) is defined as s to facilitate the analysis, which is only associated with the primary and secondary mirrors, so the magnification product of the third and fourth mirrors can be expressed as

$$\beta_T\beta_F = \frac{R_3R_4}{2R_3(s-d_{23})-d_{34}\,[2(s-d_{23})-R_3]-R_4}. \quad (16)$$

As can be seen from Eq. (16), the magnification product of the third and fourth mirrors is related not only to the vertex curvature radius of the primary, secondary, third, and fourth mirrors, but also to their distances from each other.

The focal length of the system can be expressed as the product of the combined focal length of the primary and secondary mirrors and the magnification product of the third and fourth mirrors so that the magnification adjustment of the third or fourth mirror can be converted into control of the combined focal length of the primary and secondary mirrors. The combined focal length of the system's primary and secondary mirrors is constrained by the operand EFLY; the larger the target value of the operand, the smaller is the magnification product of the system's third and fourth mirrors. As can be seen from Eq. (20), the surface type parameter of each mirror and the distance between them should be set to variables before the system is desensitized. At the same time, to increase the degree of freedom for system optimization, the quadric constant of the primary, secondary, and third mirrors should also be set as variables. Using a step-by-step approach, we increase the target value of EFLY by 50 mm each time to optimize the system. According to this idea, after several iterations of optimization, a desensitized system with better imaging quality is finally obtained. The structure of the system is shown in Fig. 11, and the MTF and spot diagram of the system are shown in Figs. 12 and 13, respectively. It can be seen from Figs. 12 and 13 that the MTF of each field of view of the system is above 0.27, and the maximum RMS spot radius of the system is 10.58 um. The relative distortion of the system is shown in Fig. 14, from which it can be seen that the maximum relative distortion of the system is 0.0453%, which meets the requirements of the design index.

B. Desensitized Design Results

The same secondary mirror disturbance as Section 3.C is imposed on the desensitization system to verify the desensitization effect of the system so that the offset of the camera image principal point and the change of the principal distance when the secondary mirror has Y- or X-eccentricity or tilt offset, and the change of the camera principal distance when the secondary

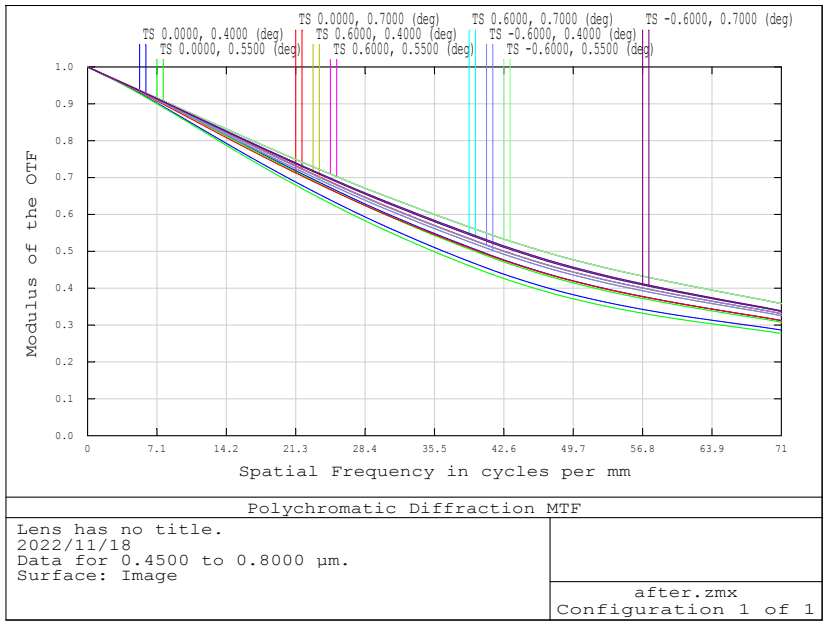

Fig. 12. MTF of the desensitized system.

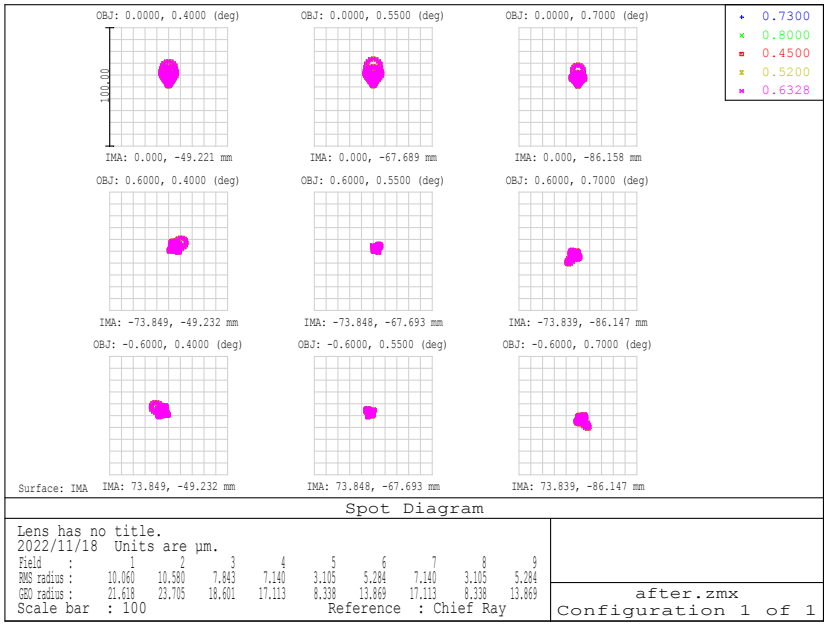

Fig. 13. Spot diagram of the desensitized system.

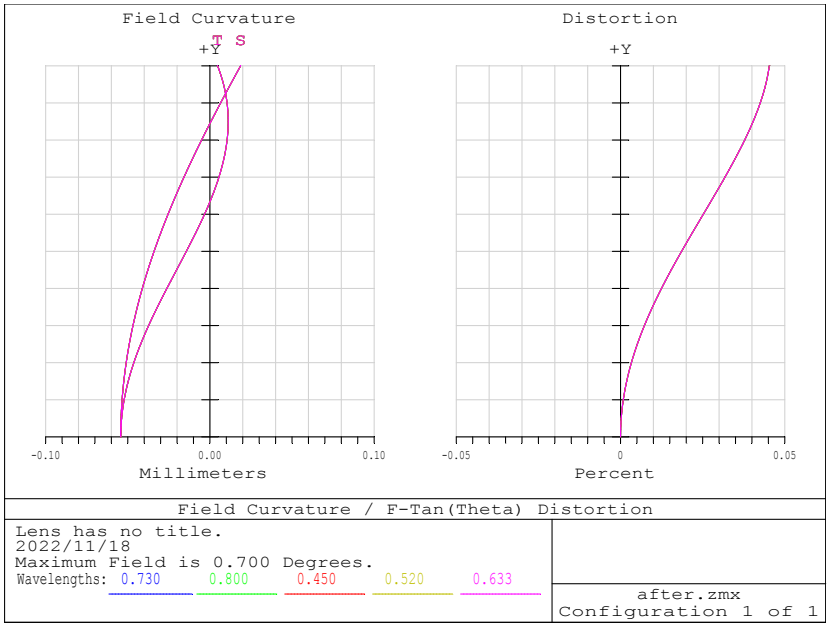

Fig. 14. Field curvature and distortion of the desensitized system.

Table 6. Analysis of the Camera Image Principal Point Desensitization Effect on the Secondary Mirror Misalignment of the Desensitized Coaxial Four-Mirror Optical System

Offset	Image Principal Point Before Desensitization/mm	Image Principal Point After Desensitization/mm	Desensitization Effect
Y/0.1 mm	0.95935916630	0.80710204144	15.87%
X/0.1°	2.30299294460	1.77530240530	22.91%

mirror have a Z-eccentricity offset. The results are shown in Tables 6 and 7.

The desensitization effect of the system can be measured by the offset of the camera image principal point and principal distance before and after desensitization. The results show that the sensitivity of the camera image principal point to the eccentricity and the tilt offset of the secondary mirror can be reduced by 15.87% and 22.91%, respectively, while the sensitivity of the camera principal distance to the secondary mirror meridian or sagittal eccentricity, tilt, and axial eccentricity offset can be reduced by 29.22%, 60.91%, and 32.95%, respectively.

Table 7. Analysis of the Camera Principal Distance Desensitization Effect on the Secondary Mirror Misalignment of the Desensitized Coaxial Four-Mirror Optical System

Offset	The Principal Distance Before Desensitization/mm	The Principal Distance After Desensitization/mm	Desensitization Effect
Y/0.1 mm	0.00006527446	0.00004619955	29.22%
X/0.1°	0.00037615429	0.00014703541	60.91%
Z/1 μm	2.14757800000	1.43986100000	32.95%

5. CONCLUSION

According to the requirements of single-line-array satellite mapping, the technical indicators of the camera were determined, and a coaxial four-mirror optical system with a focal length of 7050 mm, F-number of 10.8, field of view of 1.2°, and spectral range of 450–800 nm was designed. The imaging quality of the optical system is good, and the MTF of each field of view is better than 0.3 at the Nyquist frequency of 71l p/mm. Through the combination of mathematical modeling and ray tracing, the offset of the camera image principal point and principal distance caused by the eccentricity and the tilt offset of the system's secondary mirror was theoretically analyzed. The simulation results show that the maximum relative error does not exceed 2.119%, which proves the correctness of the theoretical analysis.

Based on the idea of adjusting the magnification of the third and fourth mirrors of the system, the system is designed to be desensitized. Through the image quality evaluation of the desensitization system, it can be seen that it has good imaging quality. By imposing different types of disturbances on the secondary mirror of the desensitization system, it can be seen that the sensitivity of the image principal point and principal distance of the camera to the secondary mirror is reduced after desensitization. Additionally, the sensitivity of the camera image principal point to the eccentricity and the tilt offset of the secondary mirror can be reduced by 15.87% and 22.91%, respectively, while the sensitivity of the camera principal distance to the secondary mirror meridian or sagittal eccentricity, tilt, and axial eccentricity offset can be reduced by 29.22%, 60.91%, and 32.95%, respectively. The result proves the effectiveness of desensitized design and provides a reference for the improvement of camera accuracy. This study can provide technical support for microsatellite mapping and has great significance for promoting the development of microsatellite mapping technology.

Funding. National Natural Science Foundation of China (51827806).

Disclosures. The authors declare no conflicts of interest.

Data availability. Data underlying the results presented in this paper are not publicly available at this time but may be obtained from the authors upon reasonable request.

REFERENCES

1. D. R. Li, M. Wang, and J. Jiang, "China's high-resolution optical remote sensing satellites and their mapping applications," Geo-Spat. Inf. Sci. **24**, 85–94 (2021).
2. Y. Yao, Y. S. Xu, and Y. L. Ding, "Optical-system design for large field-of-view three-line array airborne mapping camera," Opt. Precis. Eng. **26**, 2334–2343 (2018).
3. W. J. Cai, X. H. Zhang, F. Q. Li, J. Zheng, and S. T. Ding, "General design of space optical remote sensing camera based on high-precision surveying and mapping requirements," Proc. SPIE **11180**, 2722–2728 (2019).
4. X. M. Tang and J. F. Xie, "Overview of the key technologies for high-resolution satellite mapping," Int. J. Digit. Earth **5**, 228–240 (2012).
5. M. Wang, B. Yang, F. Hu, and X. Zang, "On-orbit geometric calibration model and its applications for high-resolution optical satellite imagery," Remote Sens. **6**, 4391–4408 (2014).
6. Y. Z. Zhang, M. T. Zheng, J. X. Xiong, Y. H. Lu, and X. D. Xiong, "On-orbit geometric calibration of ZY-3 three-line array imagery with multistrip data sets," IEEE Trans. Geosci. Remote Sens. **52**, 224–234 (2013).
7. J. S. Cao, X. X. Yuan, and J. Y. Gong, "In-orbit geometric calibration and validation of ZY-3 three-line cameras based on CCD-detector look angles," Photogramm. Rec. **30**, 211–226 (2015).
8. L. Sun, C. J. Wang, Y. H. Zhu, Y. Huang, and Y. Z. Yin, "High stability design and analysis for the dual line array camera of GF-7 satellite," Spacecraft Recovery Remote Sens. **41**, 47–57 (2020).
9. M. Isshiki, L. Gardner, and G. G. Gregory, "Automated control of manufacturing sensitivity during optimization," Proc. SPIE **5249**, 343–352 (2004).
10. M. Jeffs, "Reduced manufacturing sensitivity in multi-element lens systems," Proc. SPIE **4832**, IMC4 (2002).
11. Z. C. Qin, X. D. Wang, C. M. Ren, Y. S. Qi, and Q. Y. Meng, "Design method for a reflective optical system with low tilt error sensitivity," Opt. Express **29**, 43464–43479 (2021).
12. X. M. Cheng, Y. T. Wang, Q. Hao, and J. Sasian, "Automatic element addition and deletion in lens optimization," Appl. Opt. **42**, 1309–1317 (2003).
13. L. C. N. Scaduto, J. Sasian, M. A. Stefani, and J. C. de Castro Neto, "Two-mirror telescope design with third-order coma insensitive to decenter misalignment," Opt. Express **21**, 6851–6865 (2013).
14. Q. Y. Meng, H. Y. Wang, W. Wang, and Z. Q. Yan, "Desensitization design method of unobscured three-mirror anastigmatic optical systems with an adjustment-optimization-evaluation process," Appl. Opt. **57**, 1472–1481 (2018).
15. Q. Y. Meng, H. Y. Wang, W. Wang, Z. C. Qin, and X. D. Wang, "Sensitivity theoretical analysis and desensitization design method for reflective optical system based on optical path variation," Opt. Precis. Eng. **29**, 72–83 (2021).
16. J. Y. Miao, L. P. Zhang, and Q. W. Wu, "Design, manufacturing and assembly for optical lens of mapping camera," Opt. Precis. Eng. **16**, 1648–1653 (2008).
17. Y. Q. Xie, C. Y. Liu, S. Liu, and X. H. Fan, "Optical design of imaging spectrometer based on linear variable filter for nighttime light remote sensing," Sensors **21**, 4313 (2021).
18. Z. D. Zhang, W. B. Zheng, D. Gong, and H. Z. Li, "Design of a zoom telescope optical system with a large aperture, long focal length, and wide field of view via a catadioptric switching solution," J. Opt. Technol. **88**, 14–20 (2021).
19. D. P. Gong, J. Guo, G. L. Wang, J. G. Liu, J. M. Sun, and M. D. Shao, "Outdoor stereoscopic imaging of mapping camera with long focus off-axis three-mirror," Opt. Precis. Eng. **21**, 137–143 (2013).
20. Y. Z. Cao and W. L. Ma, "Application of two step sensitivity matrix method in Cassegrain telescope alignment," Opto-Electron. Eng. **47**, 180536 (2020).
21. X. Y. Wang, "Research on technologies of stability and calibration precision of mapping camera," Phys. Proc. **22**, 516–627 (2011).